4 Phonons and their participation in optical phenomena

Optical and thus also luminescence transitions in a semiconductor occur primarily within its electron system originating from the outer electron shells of the atomic constituents of the crystal lattice. However, interaction of the system with atomic nuclei binding the inner shell electrons is by far no negligible in optical phenomena and reveals itself in a number of effects very easy to observe. This affects the shape of the absorption edge, the width of both the absorption and emission spectral lines, gives rise to their possible fine structure, and it often results in thermal luminescence quenching, etc. In this chapter, we first recap concisely the standard facts about crystal lattice vibrations, recalling the notion of phonons. Then we mention the microscopic mechanisms responsible for interactions of excited electronic states with semiconductor lattice vibrations, the so-called exciton–phonon interaction. Next, we point out the possible local vibrations of impurity atoms. Finally, we discuss a model of the interaction between a localized optical centre and lattice vibrations (the concept of configurational coordinate) and related effects and terms: the Franck–Condon principle, thermal luminescence quenching, the Huang–Rhys factor, and weak and strong interactions with lattice.

4.1 Lattice vibrations—phonons

Atomic nuclei in a crystal keep oscillating around their equilibrium positions, determined by lattice point coordinates. The amplitudes of these oscillations rise with increasing temperature; however, they remain small compared to the lattice constant a at temperatures related to the luminescence processes (these range basically from the pumped liquid He temperature, about 1.5 K, up to room temperature of 295 K). In the simplest case of a one-dimensional crystal made of an infinite chain of identical atoms of mass m, we can write the equation of motion in the form

$$m\ddot{x}_n = -f(x_n - x_{n-1}) - f(x_n - x_{n+1}), \tag{4.1}$$

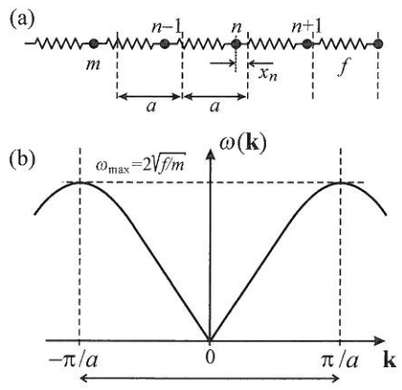

Fig. 4.1
(a) An infinite one-dimensional chain of identical oscillating atoms, and (b) the corresponding dispersion relation $\omega = \omega(\mathbf{k})$.

where x_n is the instantaneous deflection of the nth atom from its equilibrium position (Fig. 4.1(a)). In (4.1), we only consider interactions of the nearest neighbours. As a further consequence of the small amplitude of the nuclei, we can use a harmonic approximation assuming, similarly to a harmonic oscillator, that the force restoring the nuclei to their equilibrium positions depends linearly on the instantaneous deflection with the force constant (or 'spring constant') f.

It is natural to look for a solution to eqn (4.1) in the form of a wave of frequency ω, running along the chain [1, 2]

$$x_n = A\,\mathrm{e}^{\mathrm{i}\omega(t-na/c_s)} = A\,\mathrm{e}^{\mathrm{i}(\omega t-kna)}, \tag{4.2}$$

where $c_s = c_s(\omega)$ is the velocity of the wave motion, $k = |\mathbf{k}| = \omega/c_s$ is the magnitude of the corresponding wavevector $\mathbf{k}$, and A is the amplitude of the vibrations.

Similarly to other cases in wave mechanics, we are interested in the so-called *dispersion relation* for the given system, i.e. the dependence $\omega = \omega(\mathbf{k})$. We obtain it simply by substituting (4.2) into (4.1); the result is plotted in Fig. 4.1(b).

Here, several facts are worth mentioning.

(a) $\omega = \omega(\mathbf{k}) \equiv \omega_{\mathbf{k}}$ is a periodic function of k and hence it is enough to consider the range $k \in (-\pi/a, \pi/a)$ only, which is nothing but the first Brillouin zone that we encounter, in complete analogy, with the electron band structure of semiconductors.

(b) There is a maximum oscillation frequency, ω_{max}, at which the vibrations can still propagate along the chain. It follows from the solution to eqn (4.1) that $\omega_{max} = 2(f/m)^{1/2}$. This is markedly different from a continuum (represented by an oscillating string) where no such restriction on the transmitted frequency occurs.

(c) Near the centre of the Brillouin zone ($k = 0$), i.e. for $k \ll \pi/a$, the dispersion relation becomes almost linear: $\omega_{\mathbf{k}} = c_s k$. This can be easily understood. If, for $k \ll \pi/a$, we write the wavevector as $k = 2\pi/\lambda$ and combine both expressions, we get the condition $\lambda \gg a$, which means that the discrete chain structure vanishes in comparison to the wavelength.

Therefore, we are in a continuum-type situation for which, as is well known, a linear dependence governs the relationship between ω and k with c_s denoting the speed of sound.

Regarding the mechanical wave motion discussed above, we can introduce quantization, which is to a large extent analogous to the quantization of an oscillating electromagnetic field. If we restrict, as a certain approximation to reality, the number of atoms in the chain to a large but finite number, N, we can view the chain, regarding the energy, as an ensemble of N harmonic oscillators. The mean energy of a quantized harmonic oscillator $\bar{\varepsilon}$ at a given temperature T is given by the expression that constitutes part of Planck's blackbody radiation law

$$\bar{\varepsilon} = \frac{\hbar\omega_{\mathbf{k}}}{e^{\hbar\omega_{\mathbf{k}}/k_B T} - 1}. \tag{4.3}$$

Here, k_B denotes the Boltzmann constant. Thus, the energy of the entire one-dimensional crystal will be

$$\bar{E} = N\bar{\varepsilon} = \frac{N\hbar\omega_{\mathbf{k}}}{e^{\hbar\omega_{\mathbf{k}}/k_B T} - 1}. \tag{4.4}$$

We can now grasp expression (4.4) as stating that the total vibrational energy of the one-dimensional crystal is given by the sum of the energies of $N_{\mathbf{k}}$ quasi-particles, when

$$N_{\mathbf{k}} = \frac{\bar{E}}{\hbar\omega_{\mathbf{k}}} = \frac{N}{e^{\hbar\omega_{\mathbf{k}}/k_B T} - 1}; \tag{4.5}$$

we assign energy $\hbar\omega_{\mathbf{k}}$ to every quasi-particle. We call these quasi-particles—quanta of the vibrational energy of a solid—*phonons*. According to statistical physics, the statistical distribution (the distribution function) of the phonons is defined as the mean number of phonons in one quantum state. For a linear chain of N oscillating atoms, the number of allowed quantum states is equal to N [1], hence, from (4.5) we obtain for the phonon distribution function

$$n_{\mathbf{k}} = \frac{N_{\mathbf{k}}}{N} = \frac{1}{e^{\hbar\omega_{\mathbf{k}}/k_B T} - 1}. \tag{4.6}$$

Various vibrationally excited states of the crystal are characterized by different values of $n_{\mathbf{k}}$ or, in other words, each vibrational state of the lattice can be described as a state of a perfect gas of non-interacting particles—phonons. Equation (4.6) tells us that the phonons are subject to Bose–Einstein statistics and that the chemical potential of an ensemble of phonons is equal to zero. It also follows from the same equation that the phonon population depends very strongly on temperature T—as the temperature drops, the phonon population decays quickly.

The analogy to the quanta of electromagnetic radiation—photons—is rather obvious; it is, however, important to realize there is a certain difference. The expression $h\nu$ for the energy of photons holds exactly, while $\hbar\omega_{\mathbf{k}}$ for the phonons only holds in the harmonic approximation. With large amplitudes of atomic vibrations, we can no longer apply the harmonic approximation

and phonons can undergo mutual interactions. There are well-known macroscopically observable effects that cannot be explained within the context of harmonic oscillations of the lattice (e.g. the thermal expansion of solids).

Although the one-dimensional chain of identical atoms provides us with the basic concept of the phonon, it cannot encompass the full reality of a three-dimensional crystal. It is astonishing, however, that it suffices to modify the one-dimensional model just slightly to be able to represent all the basic features of vibrations in a three-dimensional crystal. This modification consists in introducing two kinds of atoms into the chain as shown in Fig. 4.2(a). We denote their masses by m and M ($m < M$). The lattice constant is then equal to $2a$ and there are two atoms per unit cell. Using an approach analogous to the previous case of identical atoms, we can formulate equations of motion for both kinds of atoms and, by solving them, we can obtain the dispersion relations shown in Fig. 4.2(b). The most important new feature as compared to Fig. 4.1 is the fact that there are now two branches of phonons separated by a frequency gap.[1] The lower branch, called the *acoustic branch*, is characterized by the relation $\lim_{\mathbf{k}\to 0} \omega(\mathbf{k}) = 0$ while on the boundary of the Brillouin zone, it has its maximum value of $\omega_{\max}^{(a)} = (2f/M)^{1/2}$. On the contrary, the upper branch, called the *optical branch*, has the highest allowed frequency in the centre of the Brillouin zone (equal to $\omega_{\max}^{(o)} = [2f(1/m + 1/M)]^{1/2}$) and the magnitude of the optical frequency gently decreases towards the boundary of the zone $k = \pm\pi/2a$ where it reaches the value of $\omega_{\min}^{(o)} = (2f/m)^{1/2}$.

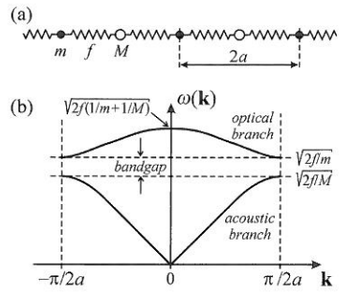

Fig. 4.2
(a) A one-dimensional chain with two kinds of oscillating atoms of masses M and m ($M > m$); (b) the corresponding dispersion relations $\omega = \omega(\mathbf{k})$.

Therefore, we speak of optical and acoustic vibrations or phonons. From the microscopic perspective, the difference between them consists in the fact that—as can be easily shown based on the equations of motion [1, 2]—light and heavy atoms move in counter-phase during optical vibrations, see also Fig. 4.5 below, while for acoustic vibrations both kinds of atoms vibrate in phase. In this case, however, even the centre of mass in each cell moves and there is a deformation wave of 'compression and expansion' travelling through the crystal, as for sound propagation. Conversely, optical vibrations—just due to the atoms moving in counter-phase—leave the centre of mass of the unit cell at rest, which allows for a non-zero frequency $\omega_{\max}^{(o)}$ even at $k = 0$. The name 'optical vibrations' stems from the fact that if there are two kinds of atoms of opposite charge per unit cell (a partially ionic bond), then the counter-phase motion means electric dipole oscillations, which can also be excited by resonance absorption of photons from the mid-infrared region.

Besides explaining the fundamental difference between the optical and acoustic vibrations, Fig. 4.2 shows several other facts that are worth emphasizing because of their importance in optical and, particularly, in luminescence phenomena:

(a) Near the first Brillouin zone boundary ($k = \pm\pi/2a$), both phonon branches are basically dispersionless, i.e. $d\omega/dk \approx 0$.

[1] Again, we can perceive a certain similarity to the electron energy band structure in semiconductors: the existence of allowed energy (frequency) bands and gaps. This is the common characteristic feature of waves propagating in periodic structures.

(b) Near the Brillouin zone centre ($k = 0$), the optical branch reveals itself dispersionless while the acoustic branch has its highest dispersion here.
(c) Figure 4.2 considers only atomic oscillations along the chain axis. These are the so-called *longitudinal vibrations*. In addition to these, however, there are also *transverse vibrations* when the atoms move perpendicularly to the chain. (Yet, in both cases, the vector $\mathbf{k}$ points in the same direction, that is, along the chain.) Therefore, we speak of transverse acoustic (TA), longitudinal acoustic (LA), transverse optical (TO) and longitudinal optical (LO) phonons.

Up to this point, we have explored only the single dimension of the linear model. It turns out that in a real three-dimensional crystal, the concept of TA-, LA-, TO-, and LO-phonons remains fully valid, but the phonon dispersion curves acquire somewhat more variable forms as against Fig. 4.2, due to numerous vibrational waves travelling through the crystal lattice in various directions featuring different electron cloud densities, different effective spring constants, etc. An example of actual phonon dispersion curves in a particular semiconductor—crystalline silicon—is shown in Fig. 4.3 [3]. Such curves are most often obtained using inelastic scattering of neutrons as they interact with phonons in various directions within a crystalline sample. These then correspond to different directions of $\mathbf{k}$ in the Brillouin zone.

Generally, in the three-dimensional case, if a crystal has n atoms per unit cell then there are exactly 3 types of acoustic vibrations characterized by the condition $\lim_{\mathbf{k}\to 0} \omega(\mathbf{k}) = 0$, and $3n$-3 types of optical vibrations with $\omega(\mathbf{k}) \neq 0$ for $k = 0$. The transverse vibrations may be doubly degenerate; the degeneration is generally removed in an anisotropic medium.

As regards Fig. 4.3, let us firstly notice that the typical phonon energy in a semiconductor is of the order of 10 meV. It is further interesting to realize that in silicon the gap between the optical and acoustic branches disappears in a certain direction in the Brillouin zone. This is due to the fact that there are two Si atoms per unit cell in the silicon (diamond) structure, and the atoms—naturally—have the same mass. According to Fig. 4.2(b), the acoustic and

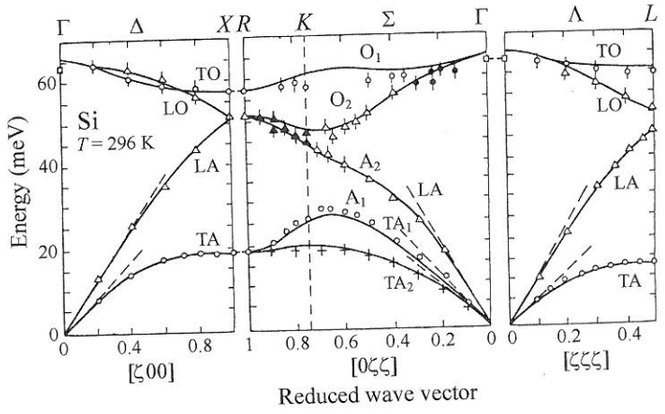

Fig. 4.3
Phonon dispersion curves of crystalline silicon in the principal directions of the Brillouin zone at room temperature. The reduced wavevector is plotted in units of $\zeta = ka/2\pi$, where a is the lattice constant. Adapted from Dargys and Kundrotas [3].

optical curves indeed coincide for $m = M$ at the boundary of the Brillouin zone.[2]

Finally, a remark on the terminology: Despite their name, acoustic phonons can participate in optical processes in a crystalline solid just like the optical phonons do! For instance, at the onset of the optical absorption edge in a semiconductor with an indirect bandgap (Si, Ge, AgBr), the type of phonons ensuring the quasi-momentum conservation law is determined by selection rules following from the symmetry of lattice vibrations, the symmetry of electron wavefunctions, and the symmetry of the corresponding matrix elements. Luminescence processes in these semiconductors are in a fully analogous situation (Subsection 7.1.4). Primarily, it is thus not of crucial importance whether the phonons are optical or acoustic. However, each of these phonon types may have a different mechanism of interaction with excited electronic states; these mechanisms are briefly treated in Section 4.2.

4.2 Electron–phonon and exciton–phonon interactions

In the preceding section, we dealt with phonons as with an isolated system. However, phonon participation in optical processes naturally requires interaction with the system of electrons responsible for the optical properties, which are basically the electrons occupying energy levels in the valence or possibly conduction band. In that case, we speak of the so-called electron–phonon interaction. Clearly, we can expect a similar type of interaction also in case the semiconductor electronic system is in an excited state and returns to the ground state, the phonon system thus participating in emission of luminescence radiation. We shall be primarily interested in this process. If, in this respect, we call the excited electronic system of the crystal an 'exciton' then we may call the corresponding interaction an exciton–phonon interaction. We shall discuss a somewhat more detailed view of the exciton–phonon and electron–phonon interactions in an excited semiconductor in Subsection 7.2.4.[3]

The following example [4] is a clear illustration of how we can imagine the charge carriers may influence the lattice vibrations. Let us consider a charge,

[2] One might then ask whether it actually makes any sense to speak of acoustic and optical vibrations in silicon if the lattice is made up of a single kind of atom. Yes, it does make sense, exactly because there are two atoms per unit cell. Then $n = 2$ and we have exactly three acoustic and $3n$–$3 = 3$ optical vibration branches. Although the optical branches cannot be excited by infrared radiation here as the bond is fully covalent, this requirement is not a condition necessary to call the lattice vibrations optical.

[3] The original meaning of the word 'exciton' in a semiconductor was clearly specified and strictly defined (Wannier, G. H. (1937). *Phys. Rev.*, **52**, 191; Elliot, R. J. (1957). *Phys. Rev.*, **108**, 1384; Nikitine, S. (1959). *Phil. Magazine*, **4**, 1) as the lowest excited electronic state of a perfect, pure crystal that can propagate freely through the lattice and transfer excitation energy (not electric charge). We shall discuss this quasi-particle, also called a Wannier 'free exciton', in connection with its important role in luminescence properties of semiconductors in Chapter 7. At a later time, the term exciton relaxed substantially from its rigour and, at present, it is used rather loosely also to denote an arbitrary bound electron–hole pair generated by light (e.g. an excited state of an impurity atom, a localized electronic excitation in an amorphous material, an electron–hole pair in a semiconductor nanocrystal, and suchlike).

whether bound or free, in a harmonically oscillating lattice made up of two kinds of ions (an ionic crystal or a semiconductor with an ionic contribution to the lattice binding energy). We shall focus on a single mode of these vibrations and we shall write its total energy (in the absence of charge that would introduce interactions) in the well-known form

$$W_0 = \frac{1}{2} m \dot{Q}^2 + \frac{1}{2} f Q^2, \tag{4.7}$$

where Q is the normal coordinate and $(f/m)^{1/2}$ denotes the angular frequency of the mode. Now we insert a charge into the lattice, which, due to Coulomb forces, introduces an additional term, $-FQ$, into (4.7), where F is the force the charge exerts on the mode. Here, we neglect higher-order terms in Q and, likewise, a possible change of the spring constant, f, due to the inserted charge. Hence, the total energy is then equal to

$$W = W_0 - F\,Q,$$

which, after introducing a new coordinate $\tilde{Q} = Q - F/f$, can be rewritten in the form

$$W = \frac{1}{2} m \dot{\tilde{Q}}^2 + \frac{1}{2} f \tilde{Q}^2 - \frac{1}{2} \frac{F^2}{f}.$$

Physically, this means a shift of the oscillator vibrations to a new equilibrium position $Q_0 = F/f$ accompanied by the release of relaxation energy $W_R = F^2/2f$, as shown in Fig. 4.4.

On the whole, there are three main microscopic mechanisms mediating the electron–phonon and exciton–phonon interactions: the deformation potential, the piezoelectric mechanism, and the Fröhlich mechanism.

The deformation potential

The energy of an electron and a hole, and thus also that of an exciton, is a sensitive function of the interatomic distance in the crystal lattice. It is well known that, for example, a deformation caused by an external force changes the bandgap value of a semiconductor. We can thus expect a similar effect to occur also due to crystal lattice vibrations. The simplest picture corresponds to long-wavelength, longitudinal acoustic vibrations when atomic displacements parallel to the direction of wave propagation occur, inducing periodic expansions and compressions of the medium on a macroscopic distance. These

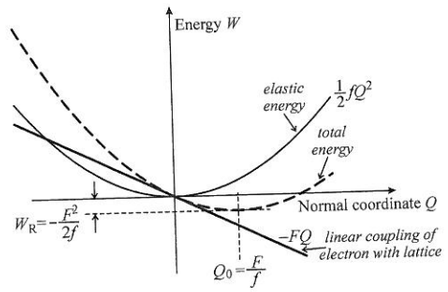

Fig. 4.4
The parabolic potential energy of harmonic oscillations in an ionic lattice, $fQ^2/2$, together with the linear coupling to the inserted electric charge ($-FQ$) result in a shift of the parabolic curve to a new equilibrium position, Q_0, and release of relaxation energy, W_R. According to Hayes and Stoneham [4].

can be expressed using the relative change in the volume of a sample, $\delta V/V$. The relative change then yields a shift in the extreme of the electron energy band $\delta E_{\mathbf{k}n}$ ($\mathbf{k}$ denotes the electron wavevector, n indexes the band). To a first approximation, the dependence reads [5]

$$\delta E_{\mathbf{k}n} = a(\mathbf{k}, n)\ (\delta V/V), \tag{4.8}$$

where $a(\mathbf{k}, n)$ is the *volume deformation potential* of the energy level $E_{\mathbf{k}n}$. It follows from this equation that the deformation potential has the dimension of energy and it is measured in eV.

However, it is neither simple to calculate such a (absolute) deformation potential theoretically nor to determine it experimentally. It is much easier to establish the difference between deformation potentials of two energy levels (the relative deformation potential). One of the commonly used experimental techniques is an optical measurement performed under external hydrostatic pressure applied to the sample. This determines the energy difference in optical transitions near the onset of the absorption edge, that is, near the extremes of the valence and conduction bands. To illustrate the situation, Table 4.1 gives the values of the relative deformation potential between extremes of the valence and conduction bands at the Γ point ($\mathbf{k} = 0$) of the first Brillouin zone. In semiconductors with a direct bandgap, this energy difference corresponds to the onset of an interband absorption edge; in semiconductors with an indirect bandgap (Si, GaP, AgBr), we in addition need to consider the deformation potential at the relevant points at the boundary of the first Brillouin zone. Table 4.1 thus also lists the available values of two absolute deformation potentials Σ_u and Σ_d, necessary to describe the energy shift according to the generalized relation (4.8) at the point $\Delta = [k/k_{max}, 0, 0]$ in the direction [100], where the conduction band minima are located in silicon and GaP.

Based on the data in Table 4.1, we can infer the following facts as regards the electron–phonon interaction. Values of the relative deformation potential given in the table decrease slightly with increasing bond ionicity, i.e. from Si towards AgBr; nevertheless, the dependence is weak and all the deformation potential values are of the same order. Therefore, this electron–phonon

Table 4.1 Deformation potentials for extremes of conduction and valence bands in selected semiconductors. The symbols $a(\Gamma_{1c})$–$a(\Gamma_{15v})$ or possibly $a(\Gamma_{15c})$–$a(\Gamma'_{25v})$ denote the relative volume deformation potential for the lowest minimum of the conduction band and the highest maximum of the valence band at the Γ point ($\mathbf{k} = 0$). Σ_d and Σ_u denote deformation potentials at the minimum of the conduction band in Si and GaP. The volume deformation potential along the [100] direction in the Brillouin zone of silicon is equal to $(\Sigma_d + \Sigma_u)$. Most data adopted from Yu and Cardona [5]. Values are given in eV.

	$a(\Gamma_{1c}) - a(\Gamma_{15v})$	$a(\Gamma_{15c}) - a(\Gamma'_{25v})$	Σ_d	Σ_u
Si		–10	5	8.77
GaP	–9.3			13
GaAs	–9			
ZnS	–4			
ZnSe	–5.4			
CdTe	–3.4			
AgBr	–2.31			

interaction mechanism has roughly the same efficiency in all semiconductors. Important from the luminescence point of view is that, in addition to mediating the coupling between electrons or excitons and the acoustic phonon field that we have mentioned several times already, both the magnitude and sign of the deformation potential have an immediate impact also on the behaviour of luminescence in semiconductors subject to a static mechanical deformation. In this sense, we must understand the data in Table 4.1 as follows.

A negative value of the relative deformation potential $a(\Gamma_{1c}) - a(\Gamma_{15v})$ means that in hydrostatic pressure experiments ($\delta V/V < 0$), the energy separation $(\Gamma_{1c}) - (\Gamma_{15v})$, i.e. the width of the bandgap, E_g, becomes larger according to (4.8). This means that, as the pressure increases in these experiments, semiconductors with a direct bandgap will show a shift in the wavelength of edge emission luminescence lines towards lower values (a 'blue-shift'). Experiments confirm this. For indirect semiconductors Si and GaP, Table 4.1 gives positive signs of the deformation potentials at the minimum of the conduction band. As the values of the deformation potential at the conduction band edge commonly turn out to be about one order of magnitude larger than at the valence band maximum, the values shown here define the character of the indirect bandgap shift and thus also that of the edge emission in Si and GaP; the applied hydrostatic pressure causes a red-shift in the edge emission here.

It should be emphasized that the account given above was considerably simplified and only applies to the long-wavelength longitudinal acoustic phonons. A more detailed discussion of the deformation potentials—additionally including also anisotropic uniaxial deformation of the crystal (or shear deformation of the TA-phonons), which lifts the degeneracy of the conduction band minima in reciprocal space of Si and Ge crystals, and the participation of *short-wavelength phonons* near the first Brillouin zone boundary in optical transitions in Si, Ge, and AgBr—can be found in [5].

An important note: The deformation potential mechanism may be partially related to optical phonons as well, particularly the long-wavelength ones ($k \ll \pi/a$). These phonons from around the centre of the Brillouin zone can also induce band edge shifts due to a relation analogous to (4.8) because a relative displacement of two ions in the unit cell induces on macroscopic distances a quickly changing local deformation (Fig. 4.5(a)), which the electron system can feel as well.

The exciton–phonon interaction due to the deformation potential occurs in all crystalline solids.

The piezoelectric mechanism

In materials of lower lattice symmetry, an electric voltage associated with a macroscopic electric field inside the material may develop, in particular between opposite sample surfaces under mechanical deformation; this is known as the piezoelectric effect. The same mechanism of generating an electric field also works in the case of deformations varying in time and resulting from the relative shift between adjacent atomic layers; that is, most

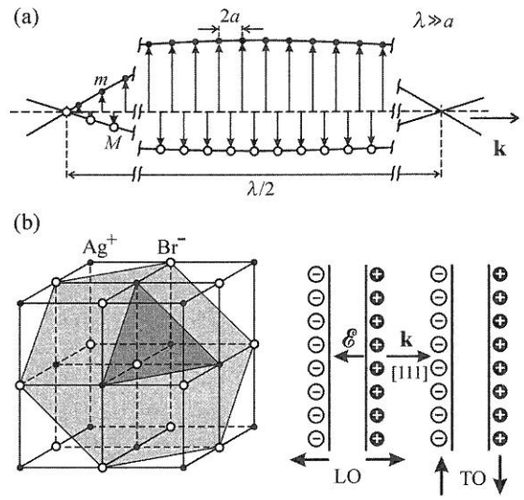

Fig. 4.5
(a) A long-wavelength TO vibration with a rather strong local deformation between adjacent atoms oscillating in counter-phase with large amplitude. (b) In a cubic crystal with the rock salt structure (e.g. AgBr), planes occupied only by positive ions alternate with planes of negative ions perpendicular to the [111] direction. LO vibrations then represent a vibrating capacitor with a constant charge but varying plate separation. This produces a varying macroscopic electric field $\mathscr{E}$ along the wave propagation direction $\mathbf{k} \parallel [111]$. TO vibrations do not possess this property. We can also imagine an analogous situation to occur in type II-VI and III-V semiconductors with partially ionic bonds.

importantly again in the case of longitudinal acoustic modes of lattice vibrations. The piezoelectric potential Φ_{PE}, describing the generated electric field, then changes the energy of a carrier of charge q, an electron or a hole, by the quantity $q\Phi_{PE}$; this is the essence of this electron–phonon coupling. Although the exciton, as a bound electron–hole pair, is electrically neutral, it is affected by the electric field, too, as the field modulates its energy levels and binding energy. Since the piezoelectric electron–phonon interaction is underlain by (long-range) Coulomb forces, the interaction is strongest for phonons with a small wavevector $\mathbf{k}$ (long wavelength), that is, for long-wavelength LA-phonons again.

This exciton–phonon interaction only occurs in crystals whose crystallographic point group does not contain the centre of inversion (in semiconducting materials, these are particularly the point groups T_d and C_{6v} that govern the crystal structure of the following materials showing significant luminescence: GaAs, GaP, GaN, CdS, CdSe, ZnO, ZnS, and ZnTe). It can be rather easily screened by free carriers and it is thus relatively weak; nonetheless, it is stronger than the deformation potential mechanism.

The Fröhlich mechanism

This is the most important exciton–phonon interaction. However, it only occurs in ionic crystals and in semiconductors with an ionic contribution to the lattice energy (also called polar semiconductors); it is thus completely absent in elemental semiconductors like Ge and Si. Its principle consists in the fact that, due to the opposite orientation of oscillations by oppositely charged ions, long-wavelength LO-phonons induce in the vibrating crystal lattice a long-range macroscopic electric field along the direction of the wavevector $\mathbf{k}$ (Fig. 4.5(b)). This field—or equivalently the macroscopic crystal polarization—again enters the Coulomb interaction with charge carriers or excitons. It is worth mentioning that TO-phonons do not produce similar crystal polarization and thus the energy of long-wavelength LO-phonons (i.e. phonons in the neighbourhood of

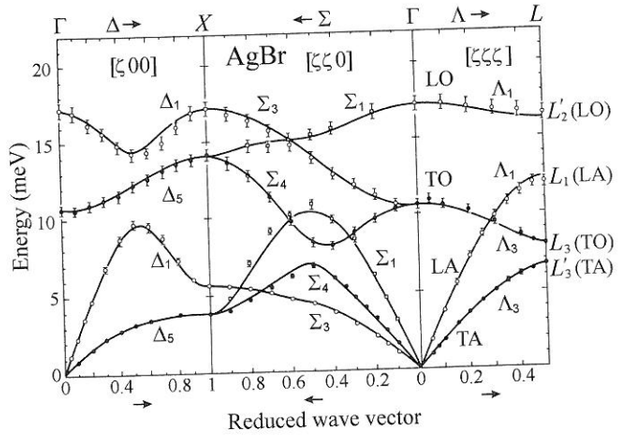

Fig. 4.6
Phonon dispersion curves in a polar semiconductor AgBr at $T = 4.4$ K. The reduced wavevector is plotted in units of $\zeta = ka/2\pi$, where a is the lattice constant. Symbols denote experimental points from neutron diffraction measurements, and lines represent the theoretical model. Symmetries of the individual phonon branches are marked by the irreducible representations of the corresponding point groups. It is particularly worth noting that at the Γ point ($\mathbf{k} = 0$), the LO-phonon energy is greater than the TO-phonon energy, which is common behaviour in polar semiconductors. Besides, however, the plot also shows some unexpected features. At the Lpoint, the energy of the TO-phonon L_3(TO) is lower than the energy of the LA-phonon L_1(LA) which contradicts the simple Fig. 4.2. This basically means that the heavier ions $M(Ag^+)$ oscillate with a higher frequency here than the lighter ones m (Br^-). This can only be explained by the effective force constants, f, being considerably different for both modes. This and related effects are discussed in more detail in Problem 4/4. The irreducible representation notation at the L point holds for a negative ion (Br^-) at the origin of coordinates. Adapted from Song and Williams [6].

$\mathbf{k} = 0$) in a polar lattice is always greater than that of TO-phonons, as illustrated, for example, by Fig. 4.6 for AgBr [6].

The Fröhlich mechanism can be well quantified using the so-called polaron coupling constant α. An electric charge in an ionic lattice polarizes its neighbourhood. The polarization involves two components: electronic and ionic. The potential at a distance r from a point charge e is screened by the dielectric constant. The electronic polarization component (the shift of the electron cloud with respect to the nuclei) and the ionic component (the shift of ions from their equilibrium positions) are jointly associated with a static dielectric constant, ε_s, that adequately describes screening at low field frequencies. The potential energy at a distance r from a point charge then reads

$$\frac{1}{4\pi\varepsilon_0\varepsilon_s}\frac{e^2}{r}$$

where ε_0 is the dielectric constant or permittivity of free space. Electric field screening by the electronic component of the lattice constituents alone is described by a high-frequency or optical dielectric constant $\varepsilon_\infty (< \varepsilon_s)$ and leads to the potential energy

$$\frac{1}{4\pi\varepsilon_0\varepsilon_\infty}\frac{e^2}{r}.$$

Ionic polarization itself, which is due to the relative motion of anions and cations (representing the mass of the vibrating lattice), is then characterized by the difference

$$\frac{e^2}{4\pi\varepsilon_0 r}\left(\frac{1}{\varepsilon_\infty} - \frac{1}{\varepsilon_s}\right).$$

Obviously, $(\varepsilon_\infty^{-1} - \varepsilon_s^{-1})$ is a crucial factor for the description of the Fröhlich mechanism of electron–phonon and exciton–phonon interactions. In practice, one introduces the above-mentioned dimensionless coupling constant α in the form [7]

$$\alpha = \frac{e^2}{8\pi\varepsilon_0 r_p}(\varepsilon_\infty^{-1} - \varepsilon_s^{-1})\ \frac{1}{\hbar\omega_{LO}}. \tag{4.9}$$

In (4.9), $r_p = \hbar/\sqrt{2m_p\hbar\omega_{LO}}$ stands for the so-called *polaron radius.* By the polaron term we denote a quasi-particle—an electron or a hole of mass m_p—that polarizes and thus locally deforms the ionic lattice as it propagates through it. This manifests itself in an increased mass of the electron or hole—as if they 'pulled' along the polarized surrounding lattice that slows them down in their motion. (We speak of an electron–polaron with a coupling constant α_e and of a hole–polaron with a constant α_h.) Thus, the effective polaron mass, m_p, is always larger than the effective mass of a 'bare' quasi-particle.

The radius r_p denotes the very size of the polarization-deformed lattice region around the charge carrier—the polaron; this is basically of the same magnitude in all polar crystals ($r_p \approx$ 1–1.5 nm). The crucial factor when characterizing the Fröhlich interaction using (4.9) is thus the value of the coupling constant, quoted for selected semiconductors in Table 4.2. As expected, the values of α_e, α_h increase with the fraction of bond ionicity (from homopolar semiconductors Ge, Si towards type I-VII semiconductors). Therefore, we can expect the strongest Fröhlich electron–phonon coupling, i.e. polaron effects, in silver halides AgBr, AgCl and in thallous halides. Experimental results confirm this reflection. However, in the case of the exciton–phonon coupling, the situation becomes somewhat different. It is expected that the exciton–phonon interaction will become stronger here, like in the case of the deformation mechanism, with increasing radius of the Wannier exciton a_x. (We can infer this on the basis of an analogy between the Wannier exciton and a free atom—the polarizability of an atom increases with its radius.) The exciton Bohr radius decreases, although not completely monotonically, with increasing bandgap E_g, as we shall discuss in Chapter 7. Thus, what comes into play here is not only the coupling constant α abut also the last column in Table 4.2. It turns out that the most prominent effects of the exciton–phonon coupling can be

Table 4.2 Polaron coupling constants α_e (electron–polaron), α_h (hole–polaron), and the bandgap width, E_g, in selected crystalline semiconductors; (i) denotes the indirect bandgap.

Semiconductor		α_e	α_h	E_g (eV)
Ge		0	0	(i) 0.745 ($T = 0$ K)
Si		0	0	(i) 1.17 ($T = 0$ K)
GaAs		0.03		1.519 ($T = 0$ K)
GaP	III-V	0.13		(i) 2.35 ($T = 0$ K)
GaN		0.4–0.5		3.49 ($T = 0$ K)
CdTe		0.39		1.606 ($T = 4.2$ K)
CdSe	II-VI	0.46		1.829 ($T = 80$ K)
CdS		0.65		2.583 ($T = 4.2$ K)
ZnS		0.71		3.78 ($T = 19$ K)
AgBr		1.6	2.8	(i) 2.7 ($T = 4.2$ K)
AgCl	I-VII	1.86	–	(i) 3.3 ($T = 4.2$ K)
TlBr		2.05	3.2	(i) 2.663 ($T = 4.2$ K)

observed in the luminescence of some II-VI compounds, in particular CdS. This is also partially due to the fact that the piezoelectric interaction here joins the Fröhlich interaction.

4.3 Lattice vibrations associated with point defects

In our considerations of phonons and their interactions with charge carriers we had, until now, always had in mind a perfect, pure crystal lattice without impurities and defects. However, we have already emphasized several times that a number of solid-state luminescence processes, very important as regards their application, are conditioned just by the presence of atomic-type impurities. It is thus in order to attempt to analyse now the influence of point defects in the crystal lattice on its vibrational properties [4].

Let us first clarify the differences in approaches used to describe perfect crystal vibrations and those of a crystal containing point defects. Firstly, as we have seen in Section 4.1, the vibrational modes of a perfect, defect-free crystal are characterized by the wavevector **k**. Secondly, these modes are fully delocalized due to the translational symmetry of the lattice. This means that, knowing the oscillation amplitude in a certain part of the crystal, we find the same oscillation amplitude—without being enhanced or damped—in any other macroscopically separated region.

We usually assume that the imperfect lattice of crystals containing point defects retains its harmonic character of vibrations and hence we may speak of its vibrational modes and phonons. Yet, we may no longer use the term wavevector and employ fully the concept of the translational symmetry of the lattice. The amplitude of the vibrational mode will be generally different in different sections of the crystal.

Let us now assume that the lattice contains a single point defect, e.g. an impurity atom of mass M' different from the masses of atoms or ions constituting the host crystal. One can imagine three different types of vibrational modes.

1. Certain crystal vibrational modes may happen not to be affected by the presence of the defect at all. If the defect atom indeed only has a different mass M' as we assumed and the harmonic force ('spring') constant, f, remains unchanged in its neighbourhood, then the modes with a node located at the impurity atom will not feel the presence of the defect. This is because the different mass will stay at rest (Fig. 4.7(a)).
2. The second type of mode can be called a *resonance mode*. If the mass M' is large (a heavy impurity atom) or the force constant f' in the neighbourhood of the impurity decreases due to a different type of interatomic bond ($f' < f$), or possibly if both effects are present simultaneously, then there appears a mode of a rather low frequency $\omega_R = (f'/M')^{1/2}$ (Fig. 4.7(b)). The frequency ω_R is usually situated within the band of allowed phonon frequencies of the unperturbed lattice and a resonance transfer of vibrational energy from the unperturbed area leads to an amplification of the local

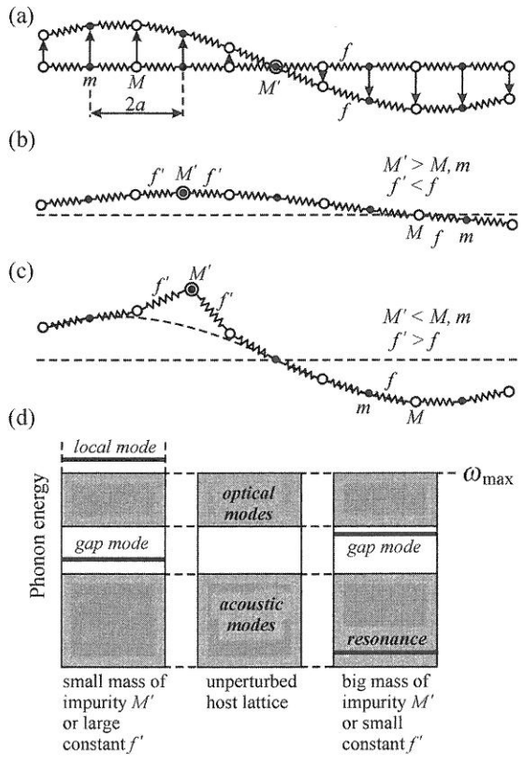

Fig. 4.7
Various types of localized vibrations of impurity atoms for the one-dimensional case: (a) an unaffected mode of the basic lattice; (b) a low-frequency resonance mode; (c) a local mode in superposition with the basic lattice mode; (d) a schematic picture of the defect modes in the energy band scheme of phonon branches.

amplitude as compared to the amplitude of vibrations in areas far away from the defect atom; hence the name resonance mode.

3. The third type of mode occurs in the neighbourhood of an impurity atom, the mass M' of which is lower than the masses of atoms in the unperturbed crystal (specifically, e.g. $M' < M$, $M' < m$ for a two-atom chain), and the neighbouring force constant f' is high, $f' > f$. The frequency of such a mode $\omega_L = (f'/M')^{1/2}$ is then located above the highest allowed frequency of perfect lattice vibrations ω_{max}. It is clear that the resonance energy transfer cannot occur here and the amplitude of such a mode decreases rather quickly away from the defect; the mode is called a *local mode* (Fig. 4.7(c)). An analogous type of defect vibration can also occur (for various ratios of the values f, f', M', M, and m) within the frequency gap between the acoustic and optical phonon branches. We can call this a *gap mode*. The frequency position of the modes discussed above in the band scheme of phonon energies is shown in Fig. 4.7(d).

It remains to assess the degree of localization of the modes under discussion in a quantitative way, if possible. The mean quadratic value of the oscillation amplitude of a given atom, in a given mode, and how this quantity varies with the distance from an impurity atom, suggest themselves to be suitable parameters. Let us assume there are N atoms oscillating in this mode, with the same amplitudes u. The potential energy $\langle V \rangle$ of N oscillating atoms in the

Table 4.3 Oscillation amplitude $\langle u^2 \rangle^{1/2}$ of various types of modes.

Mode	Close to a defect	Far from a defect	Figure
Perfect crystal mode	$\sim N_\infty^{-1/2}$	$\sim N_\infty^{-1/2}$	4.7(a)
Resonance mode	$\sim N_\infty^{-1/2}$	$\sim N_\infty^{-1/2}$	4.7(b)
Local mode	$\sim N_L^{-1/2}$	0	4.7(c)

harmonic approximation is, expressed classically, equal to $\langle V \rangle = Nfu^2/2$. At the same time, the total energy of a *quantum harmonic oscillator* (representing a given mode) is equal to $2\langle V \rangle$ and is given by relation (4.3), independent of N. Even if we add to it the zero-point energy $\hbar\omega/2$ (which is not included in (4.3)), we obtain

$$2\langle V \rangle = \frac{1}{2}\hbar\omega \coth \frac{\hbar\omega}{2k_B T}, \tag{4.10}$$

which is fully determined by the frequency ω and temperature T and is also independent of N. The only option to comply with the requirement that the expression $(Nfu^2/2)$ be independent of N is thus the scaling $\langle u^2 \rangle^{1/2} \sim 1/\sqrt{N}$. This then supplies us with information on the localization of various modes. If we denote by N_∞ the number of atoms in the host crystal and if the point defect affects the oscillation amplitude of N_L atoms in its neighbourhood then the relative values of the root mean square $\langle u^2 \rangle^{1/2}$ are given in Table 4.3.

Finally, let us note that the defect-induced vibrations modify the selection rules for infrared and Raman spectroscopy. Translational symmetry of the unperturbed crystal leads to the quasi-momentum conservation law and only optical phonons around $\mathbf{k} \sim 0$ are active in infrared spectra and Raman scattering. The presence of a defect breaks the symmetry and, therefore, modes from almost the entire Brillouin zone (with frequencies from the allowed bands) can participate in infrared and Raman experiments. At the same time, the presence of the defect itself does not appear much in the resulting spectra; they reflect primarily the phonon density of states of the perfect host crystal.

The typical impurity concentrations to which we can apply the approximation of a single isolated defect discussed above (without the need to consider defect pairs or even clusters) are of the order of 1000 ppm and less. This complies fully with the requirements for extrinsic luminescence in semiconductors, which is characterized by impurity concentrations mostly within the range 10 ppb–100 ppm.

4.4 A localized optical centre in a solid matrix—the configurational coordinate model

In the present section, we shall continue investigating the properties of a point defect (an impurity atom) in a solid. However, we shall now be primarily interested in the electronic properties of such an impurity centre related to its optical excitation and subsequent radiative transition to the ground state—

the extrinsic luminescence.[4] In Section 3.2 we gave such an optically active area in a solid the name of a *localized luminescence centre*, in order to distinguish the phenomenon from a process where emission of a luminescence photon is connected with quasi-particles moving freely through the matrix or crystal lattice (e.g. radiative recombination of a free electron–hole pair). We now introduce the concept of a configurational coordinate, which will enable us to understand how an excited luminescence centre enters into interaction with the defect modes of lattice vibrations in its neighbourhood, how the exciton–phonon interaction affects the shape of the optical spectra, and how this interaction can be quantified using optical measurements.

Let us consider an impurity atom of mass M_p embedded in a host solid; the simplest case of a one-dimensional chain with a single type of atom is shown in Fig. 4.8(a). Such a defect, as we know, leads to a distortion in the equilibrium positions of the nearest neighbours—the host atoms of mass $m \neq M_p$. Let the defect be in its ground electronic state. Let us denote by Q_{g0} the equilibrium distance between the impurity and its nearest neighbours of

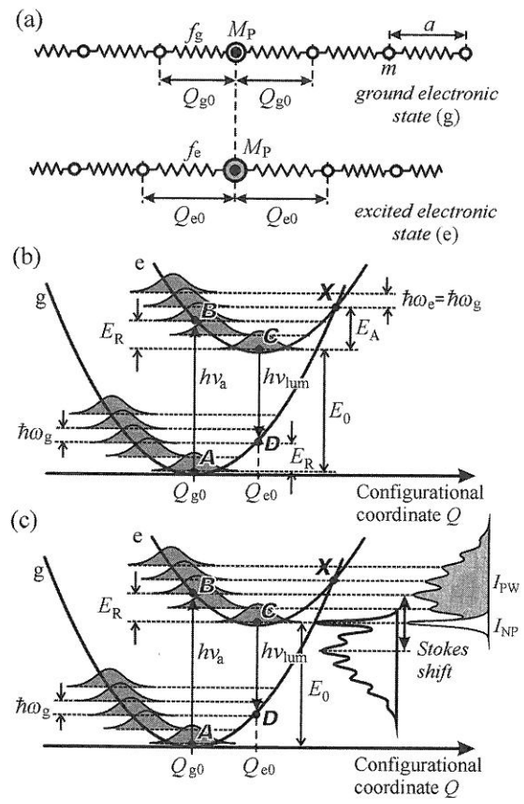

Fig. 4.8
(a) A one-dimensional chain of atoms ('matrix') containing an optically active impurity atom of mass M_p. (b) Energy of the ground (g) and excited (e) electronic states of a localized centre as a function of the configurational coordinate Q for the Huang–Rhys factor $S = 2$. (c) Schematic of the origin of optical absorption and luminescence spectra within the framework of the Franck–Condon principle at $T = 0K$. I_{NP} and I_{PW} denote the integral intensities of a no-phonon line and a phonon wing, respectively.

[4] In certain cases, the formalism discussed here can also be applied to intrinsic processes (see Problem 7/4 or the luminescence of pure AgCl in Subsection 7.2.4).

mass m; this distance generally differs from the unperturbed 'lattice constant' a, occurring sufficiently far away from the defect. The impurity atoms, just like the host atoms, oscillate around their equilibrium positions at any temperature and (assuming harmonic oscillations) we can write for the total energy of the oscillating impurity

$$E_g = E_{g0} + \frac{1}{2} f_g (Q - Q_{g0})^2. \tag{4.11}$$

Here f_g is the effective force constant determining the oscillation frequency $\omega_g = (f_g/M_p)^{1/2}$, and $(Q–Q_{g0})$ represents the instantaneous displacement from the equilibrium position Q_{g0}. We shall call Q a *configurational coordinate* and the overall situation is presented in Fig. 4.8(b). The diagram also shows the quantum-mechanical energy levels of a harmonic oscillator, represented by the oscillating atom M_p, as being equidistant with spacing $h\omega_g$. Let us remind ourselves that the quantum-mechanical probability of finding the harmonic oscillator in one of these vibronic levels reaches its highest value at the classical turning points where the corresponding vibronic level intersects the parabolic curve. Figure 4.8(b) shows this schematically, plotting the square of the modulus of the wavefunction (shaded curves). The ground vibrational state of energy $h\omega_g/2$ is an exception to this rule, with its occurrence probability highest for $Q = Q_{g0}$ (point A).

Let us now imagine the impurity atom in an excited electronic state. The classical picture is as follows: one of the valence electrons jumps to a higher energy level with a larger orbital radius; this means that the effective atom radius increases and the excited atomic 'pushes' away its nearest neighbours somewhat further off. The equilibrium distance thus grows from the value Q_{g0} to a value $Q_{e0}(> Q_{g0})$, the impurity will oscillate around a new equilibrium position, and we can write for its total energy

$$E_e = E_{e0} + \frac{1}{2} f_e (Q - Q_{e0})^2, \tag{4.12}$$

where $E_{e0} = E_{g0} + E_0$ and we usually assume that the force constant f_e remains unchanged as the atom goes to the excited electronic state, thus $f_e = f_g$. Equation (4.12) is represented by the upper parabola in Fig. 4.8(b), which, under the assumptions, arises by translating the parabola (4.11) into a new origin $[Q_{e0}, E_{g0} + E_0]$. The energy E_0 is equal to the electron excitation energy of the impurity atom and is called the *zero-phonon* or *no-phonon energy* for reasons that will become clear hereafter.

Before entering the discussion on optical transitions with Fig. 4.8 as promised, let us attempt to specify more closely the notion of the configurational coordinate Q. We introduced it by a visual demonstration—as a coordinate describing in a simple way the relative motion of a point defect and its nearest neighbours. Admittedly, such a picture very often corresponds to reality; on a more general level, however, Q may represent a configuration of multiple atoms as well as of a three-dimensional host matrix in the neighbourhood of a luminescent impurity atom or molecule. In another words, the coordinate Q is generally a combination of normal vibrational modes of a defective

periodic atomic structure. The reduction of a three-dimensional configuration to a single coordinate represents a considerable technical simplification of the problem. When introducing the term of configurational coordinate, we nowhere explicitly invoked the translational symmetry of the crystal lattice; we were only speaking of a defect atom and its immediate neighbourhood. Hence, only the short-range order is important here and the configurational coordinate model can thus be applied to both crystalline and amorphous solids.

Let us now consider how the impurity atom can be raised from the ground to an excited electronic state by absorbing a photon of visible radiation. In its ground electronic state, the system is located on the lower parabola around the minimum A. The absorption of a suitable photon proceeds extremely fast, within a time interval of about 10^{-15} s. During this time, all atoms in the solid keep their momentary positions unchanged since the typical frequencies of lattice vibrations are comparatively low, $\omega \sim 10^{12}$–10^{13}s^{-1}. Therefore, the absorption event takes place much faster than nuclei around the impurity atom can rearrange into a new equilibrium configuration and, thus, in the diagram of Fig. 4.8(b), it is represented by a vertical transition between points A and B. (Not to be confused with direct optical transitions in the Brillouin zone!) Point B, as the final transition state, is determined by that vibronic level of the excited electronic state that has the highest occurrence probability at $Q = Q_{g0}$ (the 'turning point'). Therefore, a photon of energy $h\nu_a$ equal to the energy difference between B and A is absorbed. However, point B represents an excited vibrational state of the upper energy curve, which is a non-equilibrium position. Hence, by rearranging the configuration of its adjacent nuclei, the system gradually reaches an equilibrium given by the minimum C of the upper parabola at $Q = Q_{e0}$. In addition it releases its excess energy by emitting phonons $h\omega_e(= h\omega_g)$, belonging to one of the vibrational modes associated with point defects as discussed in Section 4.3. Therefore, the ultimate outcome of the relaxation is to hand over a certain fraction of the electron excitation energy $E_R = (E_B - E_C)$ to the matrix (lattice) in the form of heat. The energy E_R is called the *relaxation energy*. At point C, the system is still in an excited electronic state of finite lifetime (10^{-9}–10^{-8} s for the allowed dipole transitions); after this time, it drops to point D of the ground electronic state, radiating a luminescence photon of energy $h\nu_{lum} = E_C–E_D$. The verticality of the transition $C \rightarrow D$ and the choice of point D are driven by the same rules as applied in the case of the absorption transition ($A \rightarrow B$). The entire process is again completed by releasing the relaxation energy equal to the energy difference between D and A (which can be easily shown to be equal to $E_R = E_B - E_C$) and returning to point A.

The approach assuming that atomic nuclei remain at rest in a solid matrix during optical excitation of the electron, and thus leading to verticality of the resulting optical transitions in the configurational coordinate diagram, is called the *Franck–Condon principle*. We can immediately see that the principle inherently explains the Stokes' luminescence law: $h\nu_a \geq h\nu_{lum}$. Thus, the localized luminescence centres are generally 'transparent' to their own emitted radiation.

Considering Fig. 4.8(b), we define several additional important terms. First of all, the two parabolic curves intersect at point X. Putting aside zero-point

oscillations, the energy separation E_A of point X from the minimum C of the upper parabola is equal to

$$E_A = \frac{(E_0 - E_R)^2}{4E_R}. \tag{4.13}$$

This is the *activation energy*, the meaning of which will be discussed in Section 4.6. Next, we usually express the relaxation energy E_R, supposing $h\omega = h\omega_g = h\omega_e$, as

$$E_R = S\hbar\omega, \tag{4.14}$$

where the dimensionless parameter S is called the *Huang–Rhys* factor. By eqn (4.14), this factor hence represents the mean number of phonons $h\omega$ emitted as the centre relaxes along the path $B \to C$ or $D \to A$. (If $\omega_e \neq \omega_g$, which is experimentally observed in certain cases, then it is basically possible to define two different values of the Huang–Rhys factor: S_e a S_g.) This factor, S, is an important indicator of the strength of coupling between the centre and the matrix. The larger the parameter S, the larger is the shift $(Q_{e0} - Q_{g0})$ and thus the stronger is the interaction between the excited centre and its surroundings. Finally, the meaning of the term zero-phonon energy for E_0 should be clearer now: it is the lowest excitation energy to be supplied to the centre to bring it to the excited electronic state. Optically, this will certainly be possible if the axes of both parabolas merge, i.e. $Q_{g0} \approx Q_{e0}$ and $E_R \to 0$, or $S = 0$. We shall show shortly, however, that this is not the only configuration in which such a transition can occur. No phonons are released during such an optical excitation and hence the term zero-phonon energy for E_0.

4.5 The shape of absorption and emission spectra of a localized centre

By making use of Fig. 4.8(b) and employing qualitative arguments, we can now proceed to get an insight into the shape of optical absorption and emission (luminescence) spectra of a localized centre. At first glance, it may seem that both the absorption and emission are formed by narrow lines corresponding to the transitions $A \to B$ and $C \to D$. The truth is, however, somewhat more complicated. The 'harmonic oscillators' of the ground as well as the excited electronic states oscillate incessantly, and so both the initial and the final point of an optical transition must respect the spatial distribution of the oscillator probability density. Thus, for instance, although an absorption transition starting from point A will most likely end at point B, it may also—with just a slightly lower probability—terminate on a vibrational level (of the excited electronic state) with an energy higher or lower by $h\omega$. Transition to the vibrational levels $\pm 2h\omega$ will even have a somewhat lower probability, etc. Obviously, even the transition with zero-phonon energy $h\nu_a = E_0$ will occur with a certain probability (which, in Fig. 4.8(b), is just the transition $-2h\omega$), and it will happen all the more so the smaller the difference $Q_{e0} - Q_{g0}$ is.

The above considerations thus lead to the following picture of the absorption spectrum: it will consist of a series of narrow lines spaced equidistantly by the phonon energy $h\omega$, and their intensities will be modulated by a certain probability distribution. Since analogous reasoning may be applied to the emission spectrum as well, only reversing the transition directions, the shape of the emission spectrum is expected to be mirror-like with respect to the absorption spectrum, both spectra sharing a common line at the zero-phonon energy E_0. All this is shown in the right part of Fig. 4.8(c).

What has been said up to now can be, naturally, represented quantitatively by calculating the transition probability [8]; it is proportional to the square of the dipole moment matrix element. Assuming independence of the dipole moment operator of the configurational coordinate Q, the spectral shape will be determined—in accordance with the above reflections—by the overlap integral of the wavefunctions of the vibrating nuclei.

At absolute zero temperature, this yields the shape of the absorption spectrum to be given by the Poisson distribution

$$I(n) \approx e^{-S} S^n / n!, \quad n = 0, 1, 2, \ldots, \tag{4.15}$$

where n numbers the vibrational level of the excited electronic state (the up-shifted parabola); as $T \to 0$ K, the transition begins from the ground vibrational level (point A) of the ground electronic state.

Figure 4.9 represents schematically several spectra of the type (4.15) for various values of the parameter S. One usually distinguishes three cases: weak ($S \leq 1$), medium ($S \approx 5$–10), and strong ($S \geq 20$) exciton–phonon coupling. It immediately follows from relation (4.15) that in the case of an extremely weak bond ($S = 0$), the spectrum will consist of a single line corresponding to the zero-phonon transition to the $n = 0$ state (the so-called *zero-phonon* or *no-phonon line*). With increasing values of S, gradually more and more lines with a higher n (the so-called *phonon replicas* or satellites) appear and the intensity of the no-phonon line $I(0) = I_{NP}$ decreases; the maximum of the spectral 'envelope' occurs roughly at $n = S$. The energy separation between the maxima of absorption and emission is called the *Stokes shift* and it is obviously given by $2Sh\omega$, as demonstrated by Fig. 4.8(c).

Figure 4.9 considers the individual lines to be infinitely narrow. In fact, the lines are already broadened at $T = 0$ K, as actually shown in Fig. 4.8(c). This happens as a result of the zero-point oscillations and other mechanisms not included in the Franck–Condon principle: homogeneous broadening due to the finite excited state lifetime and inhomogeneous broadening due to the more or less variable matrix parameters in the vicinity of any localized centre, i.e. because of possible variability in the values of energy $h\omega$. Therefore, as the parameter S increases the satellite phonon lines $n \geq 1$ gradually merge into a continuum, which is sometimes also called the *phonon wing*. Let I_{PW} denote the wing integral intensity, shown as the shaded area on the right in Fig. 4.8(c). The ratio of the no-phonon line intensity I_{NP} to the total intensity of the absorption (or emission) band $(I_{NP} + I_{PW})$ is called the *Debye–Waller factor*

$$u_{DW} = \frac{I_{NP}}{I_{NP} + I_{PW}} \leq 1. \tag{4.16}$$

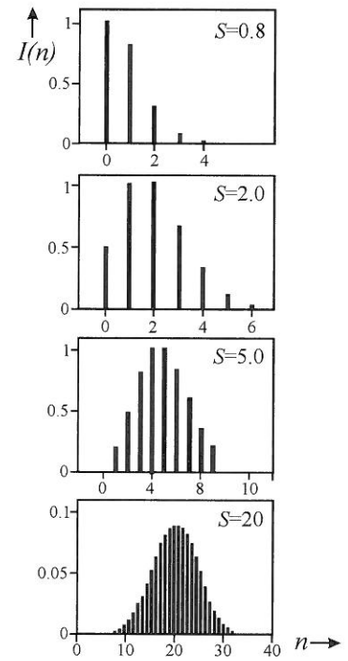

Fig. 4.9
Schematic shape of the (absorption) spectrum given by the Poisson distribution (4.15) for several values of the Huang–Rhys parameter S.

The value of u_{DW} drops quickly with increasing S as one can infer immediately from Fig. 4.9. Furthermore, it also decreases considerably with increasing temperature (here we can refer to the complete analogy with the Debye–Waller factor known from X-ray diffraction on the vibrating lattice).

Before discussing typical experimental examples, we shall briefly summarize the typical spectral features for various strengths of the exciton–phonon coupling:

- Weak coupling: a distinct no-phonon line and a negligible phonon wing, zero Stokes shift and a large Debye–Waller factor $u_{DW} \approx 1$.
- Medium coupling: an inconspicuous no-phonon line, a number of phonon satellites (up to $n \approx 10$) in the phonon wing, a small factor $u_{DW} \leq 10^{-2}$.
- Strong coupling: the no-phonon line missing completely, phonon satellites merging into a broad phonon wing, the spectrum takes the form of a broad, structureless Gaussian band with a large Stokes shift (for $n \geq 10$, the Poisson distribution turns into the Gaussian form, see Fig. 4.9), factor $u_{DW} \approx 0$.

Examples of experimental spectra are given in Fig. 4.10. We shall mainly concentrate on emission spectra since often it is not quite straightforward to measure the absorption spectrum of a localized centre in semiconductors. (Either the absorption measurements are not sufficiently sensitive as compared to the luminescence measurement, as we have mentioned already, or the absorption spectrum overlaps with the onset of the matrix absorption edge itself, and so on. In this respect, the situation is much more favourable in wide-bandgap optical materials such as alkali halides, Al_2O_3, CaF_2, CaO.)

As an example of weak exciton–phonon coupling in Fig. 4.10(a), the low-temperature (4.2 K) luminescence spectrum of phosphorus impurity atoms embedded with a concentration of $10^{16}\,cm^{-3}$ into crystalline silicon is displayed [9]. This is a pure no-phonon, narrow line ($S = 0$, $u_{DW} \approx 1$). If we give a little more thought to this observation, it may seem strange that in a semiconductor with an indirect bandgap, such as silicon, an optical recombination act without phonon participation can be found; the quasi-momentum conservation law should not enable similar processes to occur. This is a justified objection, we have not been considering a situation like this so far; in both the present section and Section 4.4, we have tacitly assumed that the semiconductor—matrix—had a direct bandgap and from this point of view, phonons were not indispensable to ensure optical transitions. Now, we really should need them; however, it is the relatively heavy phosphorus doping that breaks the perfect translational symmetry of the lattice and partially removes the ban on no-phonon transitions. We can also immediately ask the question why is it just silicon where the experiment points to a weak exciton–phonon interaction. The answer is simple. The only mechanism of this interaction in non-polar, centrosymmetric silicon is the deformation potential and the two most efficient mechanisms of this interaction, the Fröhlich and piezoelectric mechanisms, are thus missing.

An example of medium exciton–phonon coupling is displayed in Fig. 4.10(b): the low-temperature (7 K) luminescence spectrum of iodine ions I^- in a crystalline AgBr matrix [10]. We can clearly see a number of narrow phonon lines for $n = 0$ to $n = 10$, superimposed on a rather broad phonon wing.

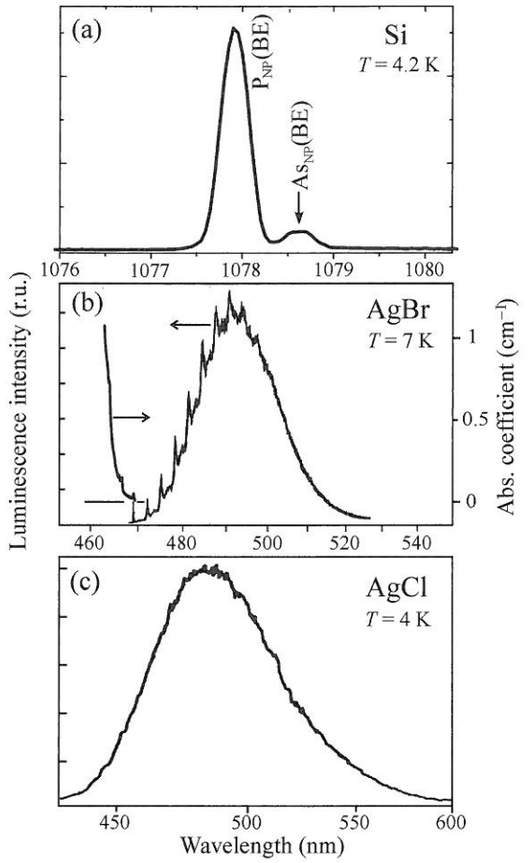

Fig. 4.10
Emission spectra of localized optical centres in semiconductors. (a) Weak exciton–phonon coupling: The (no-phonon) luminescence line of phosphorus atoms in crystalline silicon. We can also see a weak no-phonon line associated with arsenic atoms present at a lower concentration. After Pelant *et al.* [9]. (b) Medium exciton–phonon coupling: AgBr/I^- luminescence. To suppress coupling between the iodine-related I^- centre and the lattice vibrations (in order to emphasize the phonon structure), an external hydrostatic pressure was used here. After Wassmuth *et al.* [10]. The left part shows the corresponding absorption spectrum after Kanzaki and Sakuragi [11]. (c) Strong exciton–phonon coupling: luminescence of a self-trapped exciton in AgCl. After Pelant and Hála [13]. Note the different wavelength scales.

Therefore, we can estimate the values of the interaction parameters: $S \approx 8$ and $u_{DW} < 10^{-2}$ (because, although the no-phonon line is present, its intensity is minute). Also here, we notice the presence of the no-phonon line in the spectrum even though this is again the case of a semiconductor with an indirect bandgap. The reason for this is analogous to that for doped silicon. The left part of Fig. 4.10(b) also shows the onset of the absorption spectrum as measured in AgBr samples of high optical quality [11]. Comparison of the spectra confirms the correct identification of the individual lines—we can clearly see the mirror-symmetry of the spectra together with the no-phonon lines overlapping in absorption and emission. Let us again note that the presence of no-phonon lines at a localized centre in an indirect semiconductor is not commonplace. For example, $ZnSiP_2$ (with an unknown impurity as the centre) is usually cited as an indirect semiconductor where the no-phonon spectral line is missing and there is an energy separation of $2\hbar\omega$ between the onsets of absorption and emission [12].

The low-temperature (4 K) luminescence spectrum of AgCl serves as an example of strong exciton–phonon coupling in Fig. 4.10(c): a smooth, broad curve without any phonon structure [13]. Here, the localized centre

is represented by the so-called self-trapped hole in the vicinity of an Ag^+ ion, which attracts a photoelectron via Coulomb forces, thus producing the so-called self-trapped or auto-localized exciton. Its radiative annihilation then gives rise to a broadband luminescence spectrum. We shall consider these excitons in rather more detail in Subsection 7.2.4. This is an untypical *intrinsic localized centre*.

There is not much difference between the emission spectra of AgBr and AgCl apart from the total absence of both the no-phonon line and fine phonon structure in AgCl. In fact, the interaction of excitons with the lattice vibrations is very strong in both cases due to the efficient Fröhlich mechanism.

4.6 Thermal quenching of luminescence

Let us return to Fig. 4.8(b) and explore point X in more detail. At a temperature close to absolute zero, the excited centre is located near point C (and thermal vibrations are negligible). With increasing temperature T, however, the amplitude of vibrations of the centre around its position Q_{e0} increases, and, consequently, so does the chance of the system to reach point X. In solid-state physics terminology, this means overcoming the potential barrier of height E_A. The probability of such a thermally activated process is governed by the well-known relation

$$p = p_0 \, e^{-E_A/k_B T}, \tag{4.17}$$

where $p_0(s^{-1})$ is the so-called frequency factor, acquiring values of the order of the lattice vibration frequency. After reaching point X, the excited centre now has the option of a non-radiative return to the ground electronic state: at point X, it can pass over the curve of the ground state potential energy and, following the path $X \rightarrow A$ while emitting phonons, it can reach equilibrium at point A. Thus, all the energy gained via absorption of the excitation photon $h\nu_a$ is converted into the matrix vibrational energy, i.e. into heat.

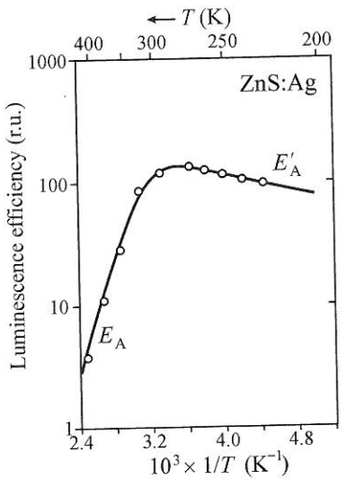

Fig. 4.11
Luminescence efficiency of ZnS:0.015% Ag as a function of temperature. Points—experiment; solid line—calculation according to (4.19) with $E'_A = 3.9$meV, $E_A = 132$meV. After Williams [14].

Realizing that the probability (4.17) is thus nothing but the probability of a non-radiative transition $p = \tau_{nr}^{-1}$ and assuming that the probability τ_r^{-1} of a radiative transition $C \rightarrow D$ is independent of temperature, the luminescence quantum efficiency (3-2) can be expressed as

$$\eta = \frac{1}{1 + \xi \exp(-E_A/k_B T)}, \tag{4.18}$$

where $\xi = \tau_r p_0$. Therefore, η drops with increasing temperature and this effect is called *thermal quenching* of the luminescence.

An example of the temperature dependence of the luminescence efficiency, established experimentally in a classical semiconductor phosphor ZnS doped with Ag (which is well-known from the Second World War era when it was used for radar screens), is shown in Fig. 4.11. This is an often-used type of graph where we plot η as a function of reciprocal temperature, $1/T$; this is because for sufficiently large T we can usually approximate (4.18) by $\eta \sim \xi^{-1} \exp(E_A/k_B T)$, and from the slope of such a logarithmic-scale plot we can immediately infer the activation energy E_A. At the same time, it can be seen in Fig. 4.11 that the thermal quenching only occurs here for temperatures $T \geq 310$ K (i.e. for $1000/T \leq 3.2$ K^{-1})—hence, this phosphor radiates most at room temperature which is highly unusual and which explains why the material is so attractive as regards its applications. It is thus obvious that relation (4.18) does not fully grasp the overall form of the experimental dependence since, when temperature increases from about 200 K to approximately 280 K, the luminescence efficiency does not drop but grows instead. A similar increase is generally observed quite often and the simple configurational coordinate model, as discussed above, can no longer encompass this fact. In order to describe the experimentally found temperature dependence η, eqn (4.18) is sometimes modified by adding another factor that describes a weakly thermally activated process resulting in an increase of the radiative transition probability. For example, the experimental points in Fig. 4.11 can be very well fitted by the equation

$$\eta \sim \frac{T \, e^{-E'_A/k_B T}}{1 + \xi \, e^{-E_A/k_B T}} \tag{4.19}$$

(see the curve in Fig. 4.11 with $E'_A \approx 3.9$ meV and $E_A \approx 132$ meV) [14]. However, in this case, it is just a phenomenological model while currently there are already more exact models based on microscopic concepts. Let us emphasize, however, that any such increase in luminescence intensity with increasing temperature is only temporary and, ultimately, thermal quenching always prevails and luminescence thus fades away completely.

And finally a note regarding the relative position of points B and X in Fig. 4.8(b). Our analysis of thermal quenching was based on the assumption that the intersection point X is at a higher energy than point B. If both points are located on the same level or if X is even lower than B then there will be a steep drop in luminescence intensity since a non-radiative transfer of the electronic excitation energy to the matrix will prevail already at very low temperatures.

4.7 Problems

4/1: Show that the vibrational energy of a one-dimensional 'crystal' with N atoms is at high temperatures ($\hbar\omega_k \ll k_B T$) equal to $\bar{E} = N k_B T$. (Hint: Transform relation (4.4) into the form

$$\frac{\bar{E}}{k_B T} = \frac{N\hbar\omega_k}{k_B T} \left[\exp\left(\frac{\hbar\omega_k}{k_B T} \right) - 1 \right]^{-1}.)$$

4/2: Show that the total energy of a harmonic oscillator in quantum physics is equal to $(\hbar\omega/2)\coth(\hbar\omega/2k_B T)$.

4/3: Prove that in the harmonic approximation and assuming $f_e = f_g$, the relaxation energies E_R in Fig. 4.8(b) in the ground and excited electronic states are the same. Show that the activation energy E_A is given by eqn (4.13).

4/4: The lattice vibrations in crystalline silver bromide show a number of peculiarities. This is caused by the deformability of the Ag^+ ion and the considerable fraction of both ionic and covalent bonds in the crystal.

These effects lead to very dissimilar force constants for different vibration types, to a low energy of TO-phonons at the L point (Fig. 4.6), and to the inverted character of TO- and TA-phonons near the L point. Discuss these phenomena according to Dorner *et al.* [15].

4/5: Confirm that at $T = 0\,\mathrm{K}$ the Debye–Waller factor u_{DW} and the Huang–Rhys factor S are related by $u_{\mathrm{DW}} = \exp(-S)$. (Hint: Use eqns (4.15) and (4.16).)

References

1. Dekker, A. J. (1963). *Solid State Physics*. Chap. 2. Prentice-Hall, Englewood Cliffs, N.J.
2. Peyghambarian, N., Koch, S. W., and Mysyrowicz, A. (1993) *Introduction to Semiconductor Optics*. Chap. 4. Prentice Hall, Englewood Cliffs, N.J.
3. Dargys, A. and Kundrotas, J. (1994). *Handbook on Physical Properties of Ge, Si, GaAs and InP*. Science and Encyclopedia Publishers, Vilnius.
4. Hayes, W. and Stoneham, A. M. (1985). *Defects and Defect Processes in Non-metallic Solids*. Chap. 1. John Wiley, New York.
5. Yu, P. Y. and Cardona, M. (1996). *Fundamentals of Semiconductors*. Springer, Berlin.
6. Song, K. S. and Williams, R. T. (1996). *Self-Trapped Excitons* (Springer series in solid state sciences Vol. 105). Springer, Berlin.
7. Böer, K. W. (1990). *Survey of Semiconductor Physics*. Van Nostrand Reinhold, New York.
8. Vij, D. R. (ed.) (1998). *Luminescence of solids*. Plenum Press, New York; Yamamoto, H. (1999). *Fundamentals of Luminescence*. In *Phosphor Handbook* (ed. S. Shionoya and W. M. Yen), p. 35. CRC Press, Boca Raton.
9. Pelant, I., Hála, J., Ambrož, M., Vácha, M., Valenta, J., Adamec, F., Kohlová, V., and Matoušková, J. (1990). *Impurity assessment in Si wafers by photoluminescence method V*. Research report for Tesla Rožnov. Charles University in Prague, Faculty of Mathematics & Physics, Prague.
10. Wassmuth, W., Stolz, H., and von der Osten, W. (1990). *J. Phys. C: Cond. Matter*, **2**, 919.
11. Kanzaki, H. and Sakuragi, S. (1969). *J. Phys. Soc. Japan*, **27**, 109.
12. Shah, J. (1972). *Phys. Rev. B*, **6**, 4592.
13. Pelant, I. and Hála, J. (1991). *Solid State Comm.*, **78**, 141.
14. Williams, F. E. (1948). *The mechanism of rate processes in the luminescence of solids*. In *Preparation and Characteristics of Solid Luminescent Materials*. Cornell Symposium 1946, p. 337. John Wiley, New York; Chapman & Hall, London.
15. Dorner, B., von der Osten, W., and Bührer, W. (1976). *J. Phys. C: Solid State Phys.*, **9**, 723.

Channels of radiative recombination in semiconductors

5

Various radiative recombination processes have already been mentioned several times in the previous chapters. These processes were, however, not discussed from the point of view of the underlying physics; more emphasis was put on the introduction (or reminder) of the basic concepts and terminology, which will be indispensable later in the book. The configurational coordinate model, which was described in the previous chapter, for example, is broadly applicable. In this chapter, we are going to show in which particular aspects of luminescence in semiconductors the application of this model is completely straightforward, when, on the other hand, it does not make any sense at all, or when it can be used only formally and with prudence.

Now that everything is ready we can move on to giving systematic explanations of known channels of radiative recombination in semiconductors. First, we will list an overview of these channels. Secondly, we will focus in more detail on the spectral shape of the emission line of recombining free electron–hole pairs, and of related recombinations of a free electron with a neutral acceptor or a free hole with a neutral donor. Then we will talk about the shape of the emission spectra of recombining donor–acceptor pairs and finally we will mention the particularity of exciting luminescence via a two-photon absorption process.

5.1 Overview of luminescence processes in crystalline semiconductors

Let us start with the widely accepted classification of luminescence processes according to the intensity of excitation. The *low-fluence* or *weak excitation* processes (i.e. taking place when a gas-discharge lamp, an incandescent lamp or a continuous-wave gas laser with the output power of the order of 0.01–$10\,\mathrm{W/cm^2}$ are used for excitation) comprise:

- radiative recombination of free excitons (often denoted as FE for a free exciton, or X);
- radiative recombination of free excitons with simultaneous emission of an LO phonon (FE–LO, X–LO);